EUROPEAN ORGANIZATION FOR NUCLEAR RESEARCH
ORGANISATION EUROPEENNE POUR LA RECHERCHE NUCLEAIRE

CERN - PS DIVISION

PS/ DI/ Note 99-06
AD Note 047

# BEAM EVOLUTION IN THE ANTIPROTON DECELERATOR (AD) UNDER THE INFLUENCE OF RESIDUAL GAS AND INTRA BEAM SCATTERING

N. Madsen

Geneva, Switzerland
18 February 1999

# Contents

# Chapter I

# Introduction

When operational for users in late 1999 the Antiproton Decelerator (AD) is supposed to decelerate anti protons created at a momentum of 3.5 GeV/c to a momentum of 0.1 GeV/c. The antiproton decelerator is build as a reconfiguration of the former Antiproton Collector (AC). As the AC was mainly run with antiprotons at an energy of 3.5 GeV/c several changes to the machine are being done to accomodate the change in cycle scheme to the AD cycle. When decelerating a charged particle beam the effects of scattering on the rest gas, intra beam scattering as well as space charge tune shifts increase. To compensate for the beam blow up due to these effects the AD cycle includes a couple of flat tops at different energies where beam cooling will be activated. The AD cycle as shown in the design report [1] is reproduced in figure 1.1.

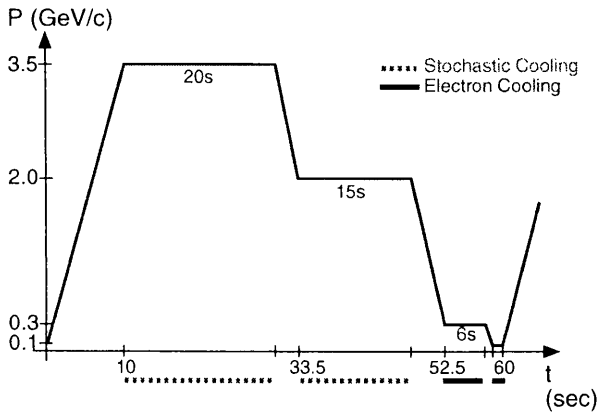


Figure 1.1: Standard AD cycle as described in the design report [1].

In this report we present theoretical calculations done in order to evaluate the equilibrium beam emittances and momentum spreads at the two low energy flat tops in the cycle (figure 1.1). We also discuss the beam development during the deceleration from 0.3 GeV/c to 0.1 GeV/c. The aim of this study is to understand what mechanisms are important for the beam development during these phases.

Ignoring resonances there are three contributing elements to the beam evolution in the AD, which are of interest. The three elements are the beam interaction with the residual

gas in the vacuum chamber, the intrabeam scattering and the electron cooling to be applied at the flattops. For electron cooling it is rather complicated to make resonable estimates. Thus in this report that part of the study has been left out. Instead we concentrate on the deteriorating effects of the residual gas and the intrabeam scattering.

The desired beam characteristica for the two low energy flat tops in the AD cycle as given in the design report [1] are reproduced in table 1.1.

| p | $\epsilon_i$ | $\epsilon_f$ | $\Delta p/p_i$ | $\Delta p/p_f$ | t |
|---|---|---|---|---|---|
| [GeV/c] | [$\pi$ mm mrad] | | [%] | | [sec] |
| 0.3 | 33 | 2 | 0.2 | 0.1 | 6 |
| 0.1 | 6 | 1 | 0.3 | 0.01 | 1 |
| [GeV/c] | [m/s] | | [m/s] | | [sec] |
| 0.3 | $9.9{\cdot}10^4$ | $2.4{\cdot}10^4$ | $4.6{\cdot}10^4$ | $2.3{\cdot}10^4$ | 6 |
| 0.1 | $1.5{\cdot}10^4$ | $0.6{\cdot}10^4$ | $2.4{\cdot}10^4$ | $7.9{\cdot}10^2$ | 1 |

Table 1.1: Design Study: Transverse emittances and momentum spread before (i) and after (f) electron cooling, and cooling times. Only the adiabatic increase due to deceleration is considered[1][1]. For easier comparison later on we have added the corresponding ($1\sigma$) thermal velocities.

The final emittance of 1 $\pi$ mm mrad at 0.1 GeV/c is given by the needs of the experiments.

[1] $2\sigma$ emittances [$\epsilon = (2\sigma)^2/\beta$] and $4\sigma_p$ momentum spread [$\Delta p = 4\sigma_p$] are used throughout this report.

# Chapter II

# Residual Gas Effects

In the former AC the scattering on the residual gas was not a big problem, as the lifetimes were of order tens of hours. The pressure in the AC was of the order of $8.0{\cdot}10^{-7}$ Pa (= $6.0{\cdot}10^{-9}$ Torr). However, as we will see in this chapter, it turns out that at low energy the scattering on the residual gas becomes an important cause for losses as well as heating of the beam.

Therefore, calculations taking into account how these cross sections and thus lifetimes scale with the pressure and beam momentum are important for the determination of the equilibrium beam properties in the AD, and necessary in order to estimate how much improvement of the vacuum is needed. This has been done in the AD design report [1] and in detail in the notes [2] and [3], and the calculations as well as conclusions are reproduced here for completeness, including some new additions. All calculations are done with the desired AD vacuum which is 20 times better than in the former AC, i.e. with a pressure of $4.0{\cdot}10^{-8}$ Pa (= $3.0{\cdot}10^{-10}$ Torr). The "standard composition" of the residual gas used for these calculations is the composition earlier measured in the AC, listed in table A.1.

## 2.1 Introduction

Following the lines of [4] and [5], we consider three important contributions to beam loss and heating due to interaction with the residual gas:

- Nuclear Scattering.
- Single Coulomb Scattering.
- Multiple Coulomb Scattering.

We first calculate the magnitude and scaling of these contributions, including the composition of the residual gas (called the vacuum composition, which is discussed in some detail in appendix A). The lifetime due to these contributions is then compared with the time scale of the AD cycle, and the beam blow up is compared with the acceptance of the AD machine. Included is also a study of how critically the vacuum composition will influence these results.

## 2.2 Nuclear Scattering

A proton involved in a nuclear scattering event (nuclear reaction or diffraction scattering) can be assumed to be scattered into so large angles or loose so much energy that it is lost from the beam. This will result in a simple exponential decay

$$I_n(t) = I_0 \exp\left(-\frac{t}{\tau_n}\right) \tag{2.1}$$

where

$$\tau_n = \frac{1}{\beta c n_a \sigma_a} \tag{2.2}$$

Here $\beta c$ is the beam velocity, $n_a$ is the number of atoms per unit volume, and $\sigma_a$ is the nuclear scattering cross section.

The nuclear scattering cross section for the AD momentum range can be approximated by using the results of [6] and [7].

$$\sigma_a = A^{2/3}\left(\frac{53}{p[GeV/c]} + 66\right) \text{mbarn} \tag{2.3}$$

then, for convenience, we define a nuclear scattering equivalent density $n_{ns}$(as we in [2] defined a multiple scattering equivalent density) which is given as follows

$$n_{ns} = \sum n_i A_i^{2/3} \tag{2.4}$$

resulting in the following expression for the nuclear scattering life time

$$\tau_{ns} = \frac{1}{\beta c n_{ns} \sigma_{ns}} \tag{2.5}$$

where $\sigma_{ns}$ is the Hydrogen cross section (A=1).

Using the vacuum description from [2], which is repeated in appendix A, we obtain a total nuclear scattering equivalent density of $6.4{\cdot}10^{13}\text{m}^{-3}$, and a nuclear scattering lifetime in the AD as plotted in figure 2.1.

$$\tau_{ns} = \frac{1.45 \cdot 10^5 \text{ hours}}{\beta\,(53/(p[GeV/c]) + 66)} \tag{2.6}$$

## 2.3 Single Coulomb Scattering

Beam loss due to Coulomb scattering occurs when a beam particle is deflected in a collision with the residual gas by an angle which brings it outside the ring acceptance. Integrating the Rutherford cross section we obtain an expression for the cross section for scattering by an angle larger than $\theta$ [8]

$$\sigma_{sc} = 4\pi\left(\frac{Ze^2}{4\pi\epsilon_0\gamma m_p c^2\beta^2}\right)^2 \frac{1}{\theta^2} \tag{2.7}$$

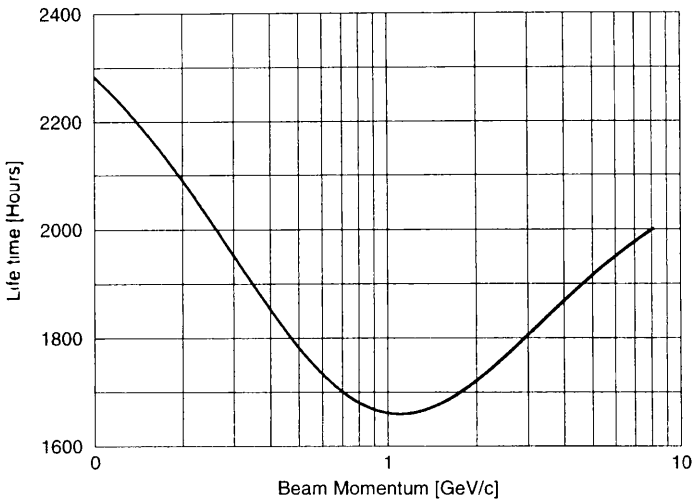


Figure 2.1: Lifetime in the AD due to nuclear scattering.

where $Z$ is the charge of the rest gas nucleus, $\gamma$ and $\beta$ relativistic factors, and $m_p$ the rest mass of the proton. The minimum angle causing loss of a particle is described by the machine acceptance, for the AD the horizontal and vertical acceptances are about the same, thus we have to use an 'average' angle as calculated in [9]

$$\frac{1}{\theta^2} = \frac{1}{2\theta_H^2} + \frac{1}{2\theta_V^2} \quad ; \quad \frac{1}{\theta_{H,V}^2} = \frac{\beta_{H,V}}{\epsilon_{accep,H,V}} \tag{2.8}$$

where $\beta_{H,V}$ are the average beta functions ($\beta_H \sim 7.5$ m and $\beta_V \sim 7.0$ m for the AD lattice). Inserting this into equation (2.7) and using equation (2.2) we obtain the beam life time due to single Coulomb scattering

$$\tau_{sc} = \frac{\gamma^2\beta^3\epsilon_{accep}}{2\pi r_p^2 c\beta_z n_{sc}} \tag{2.9}$$

where we for convenience have introduced the classical proton radius $r_p$=1.535·$10^{-18}$ m and the single Coulomb scattering density $n_{sc}$ given by :

$$n_{sc} = \sum Z_i^2 n_i \tag{2.10}$$

which for the standard vacuum conditions in the AD (appendix A) equals $n_{sc}$ = 3.18·$10^{14}$ $m^{-3}$.

Inserting the single Coulomb scattering density using a ring acceptance of $\epsilon_{accep}$ = 150 $\pi$ mm mrad from [2], and the average beta function for the AD we obtain the following expression for the single Coulomb scattering lifetime

$$\tau_{sc} = 2040 \text{ hours} \cdot \beta^3\gamma^2 \tag{2.11}$$

which has been plotted on figure 2.2.

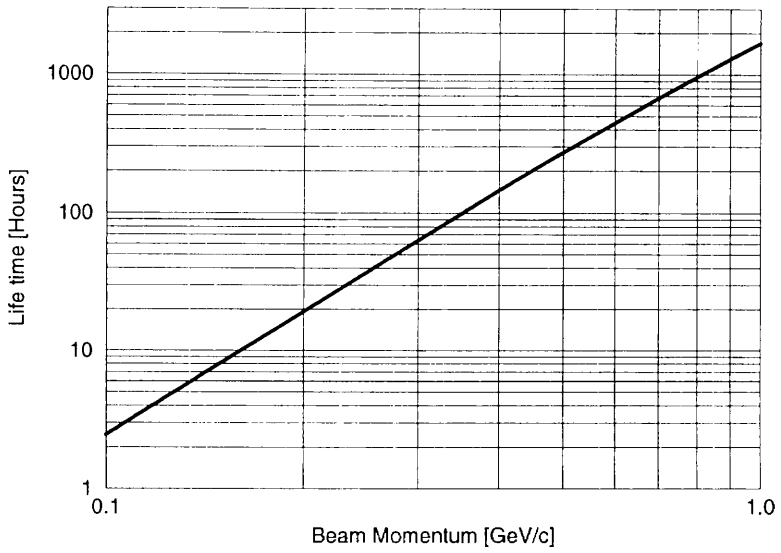


Figure 2.2: Single Coulomb Scattering lifetime in the AD with standard vacuum conditions (appendix A) as a function of beam momentum. An acceptance of 150 $\pi$ mm mrad has been assumed.

## 2.4 Multiple Coulomb Scattering

In multiple Coulomb scattering we consider the small angle scattering events which were ignored in the single Coulomb scattering losses as these do not directly lead to beam loss. The small angle scattering however leads to a blow up of the beam, which, if not counteracted by cooling, eventually will lead to losses due to the constraints given by the acceptance of the machine.

### 2.4.1 The cross section

Following the line of thinking in [4] we assume pure Coulomb scattering. Thus we can use the Rutherford cross section. For small scattering angles this can be written :

$$\frac{d\sigma}{d\vartheta}(\theta) = 8\pi Z^2 r_e^2 \left(\frac{m_e c^2}{\beta c p}\right)^2 \theta^{-3} \tag{2.12}$$

where $Z$ is the charge of the scattering atoms (the incoming particle is assumed to be a proton), $r_e$ is the classical electron radius, $m_e$ the electron mass, $p$ the momentum of the scattered proton and $\beta$ the velocity in units of light speed. This formula is only valid in a limited angular range. We will assume it is zero outside this range.

The minimum angle $\theta_{min}$ is defined by the screening effect of the electron shells of the

atom :

$$\theta_{min} = \alpha Z^{1/3} \frac{m_e c^2}{\beta c p} \tag{2.13}$$

the maximum is given by

$$\theta_{max} = \frac{280}{A^{1/3}} \frac{m_e c^2}{\beta c p} \tag{2.14}$$

where $\alpha$ is the fine structure constant.

### 2.4.2 In free space

If a beam of particles moves through a residual gas at some velocity $v$, the mean square angular deflection rises linearly with time

$$\theta^2_{rms}(t) = n_a \beta c t \int_0^\pi \theta^2 \frac{d\sigma}{d\theta}(\theta) d\theta \tag{2.15}$$

this expression is equivalent to diffusion in the two dimensional space of the projected scattering angles $\theta_z$ and $\theta_x$, which are the two perpendicular components which spans the plane perpendicular to the beam direction. Thus each of these scattering angles increases with half the mean square of $\theta$

$$\theta^2_{z,rms} = \frac{1}{2}\theta^2_{rms} \tag{2.16}$$

### 2.4.3 In a focusing field

In the focusing field of a storage ring an angular deflection will be 'converted' to an increase in the betatron amplitude according to the beta function at the position of the event. To ease calculations we average the beta function over the circumference. We will furthermore assume that the two transverse dimensions are uncoupled.

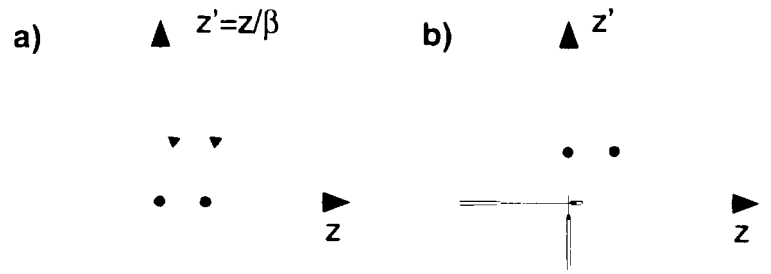


Figure 2.3: Transverse Phase Space. Two different particles gets the same angular kick by collision with rest gas, this results in an increase in the rms spread of the beam at this position.

As seen on figure 2.3 the angular spread induced by multiple scattering will lead to an increased beam size (and emittance). On average the increase in the beam emittance by scattering is given by[1] [13] :

$$\epsilon = \frac{1}{2}\theta^2_{z,rms} \cdot \beta \tag{2.17}$$

Thus for a storage ring we obtain the following expression for the time development of the beam emittance in each transverse plane :

$$\begin{aligned}
\epsilon_z(t) &= \epsilon_{z0} + \frac{1}{4}\theta^2_{rms}(t) \cdot \beta_z \\
&= \epsilon_0 + \frac{1}{4}\beta_z n_a \beta c t \int_0^{\pi} \theta^2 \frac{d\sigma}{d\theta}(\theta) d\theta \\
&= \epsilon_0 + \frac{1}{4}\beta_z n_a \beta c t \int_{\theta_{min}}^{\theta_{max}} \theta^2 8\pi Z^2 r_e^2 \left(\frac{m_e c^2}{\beta c p}\right)^2 \theta^{-3} d\theta \\
&= \epsilon_0 + 2\pi\beta_z n_a r_e^2 \frac{(m_e c^2)^2}{\beta c p^2} Z^2 \ln\left(\frac{\theta_{max}}{\theta_{min}}\right) t \\
&= \epsilon_0 + 2\pi\beta_z n_a r_e^2 \frac{(m_e c^2)^2}{\beta c p^2} Z^2 \ln\left(\frac{\alpha^{-1} \cdot 280}{(A \cdot Z)^{1/3}}\right) t
\end{aligned} \tag{2.18}$$

where we note that the emittance growth depends on the residual gas composition. The vacuum composition is discussed in Appendix A, and in table A.1 the composition for the AC is listed. To incorporate this dependence we introduce the gas factor $G$ :

$$G = Z^2 \ln\left(\frac{\alpha^{-1} \cdot 280}{(A \cdot Z)^{1/3}}\right) \tag{2.19}$$

as the densities of the various composites are not equal it is often easier to define a compensated molecular density of the gas (it is an approximation to add contributions from atoms in molecules as if they were free), defined below

$$n_{ms} = \sum_i n_i \cdot \frac{G_i}{C_{ms}} \; ; \; C_{ms} = \ln(\frac{280}{\alpha}) \tag{2.20}$$

where the constant $C_{ms}$ has been introduced such that the multiple scattering density for Hydrogen atoms (A=1 and Z=1) is the same as the actual density of atoms.

Using the values from table A.1 we obtain for the AD vacuum conditions (20 times improvement of AC vacuum) a multiple scattering density of $n_{ms} = 2.76 \cdot 10^{14}$ m$^{-3}$.

With the definition of the multiple scattering density, the expression for the emittance growth simplifies to

$$\epsilon_z(t) = \epsilon_0 + 2\pi\beta_z n_{ms} C_{ms} r_e^2 \frac{(m_e c^2)^2}{\beta c p^2} t \tag{2.21}$$

[1] This, more exact expression, differs by a factor $\frac{1}{2}$ from the approximation used in [2].

Now the emittance ordinarily used in discussions on the AD is the 2 sigma emittance ($\epsilon_2 = (2\sigma)^2/\beta$), thus the above expression should be multiplied with a factor of 4 to compensate :

$$\epsilon_{2,z}(t) = \epsilon_{2,0} + 8\pi\beta_z n_{ms} C_{ms} r_e^2 \frac{(m_e c^2)^2}{\beta c p^2} t \tag{2.22}$$

inserting in this equation, using an average $\bar{\beta}_z$=7.0m (AD), we obtain :

$$\epsilon_{2,z}(t) = \epsilon_{2,0} + \frac{3.17 \cdot 10^{-4}\ \pi \text{ mm mrad}}{\beta(p[GeV/c])^2} t[s] \tag{2.23}$$

the growth rate is illustrated on figure 2.4.a.

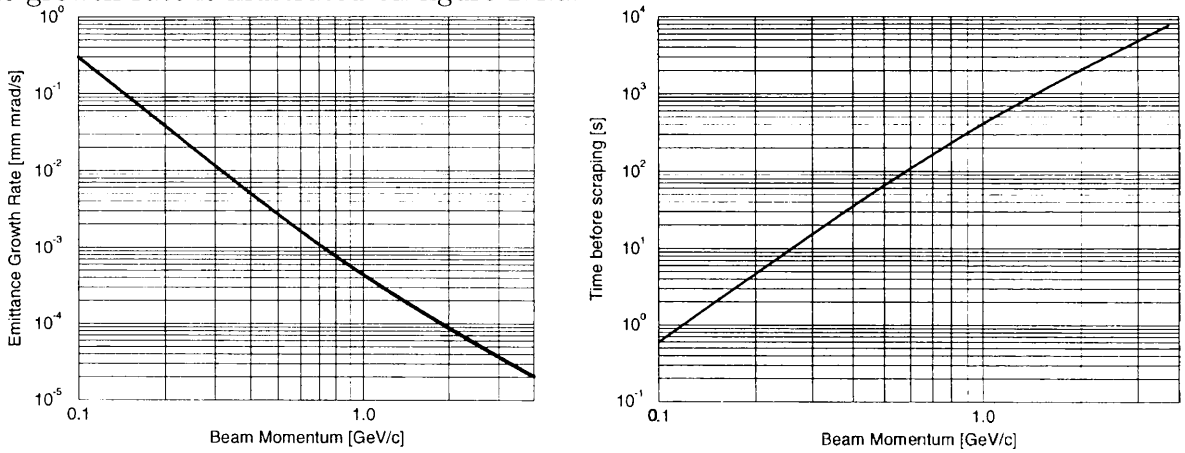


Figure 2.4: a) Emittance growth rate due to multiple scattering as a function of beam momentum. b) The time it takes before multiple scattering has blown the beam up enough to hit the aperture of the vacuum chamber (starting from 6 $\pi$ mm mrad). Both cases for the standard AD vacuum conditions (i.e. AC vacuum composition and a Nitrogen equivalent pressure of $4.0 \cdot 10^{-8}$ Pa) with an average focusing function $\bar{\beta}_z$=7.0 m).

Of course the beam can not be allowed to expand forever, as the vacuum chamber defines a finite available aperture. Following [5] we take the available acceptance to be $\epsilon_{accep} = 150\ \pi$ mm mrad. The beam will start to be lost when the beam halo hits the chamber walls. We define the halo as extending to 6 sigma of the beam size.

A Gaussian beam with a 6 sigma area $\epsilon_{accep} = 150\ \pi$ mm mrad corresponds to a Gaussian beam with a 2 sigma emittance area of $\epsilon_{2,accep} = 16.7\ \pi$ mm mrad. We thus have the following expression for the time it takes before the beam starts being scraped :

$$t_{scraped}(p) = \frac{\epsilon_{2\,accep} - \epsilon_{init}}{3.17 \cdot 10^{-4}\ \pi \text{ mm mrad}} \cdot \beta(p[GeV/c])^2 \cdot \text{s} \tag{2.24}$$

inserting numbers, and using that the initial emittance at 0.1 GeV/c is supposed to be 6 $\pi$ mm mrad (table 1.1), we obtain

$$t_{scraped}(p) = 560 \cdot \text{min} \cdot \beta(p[GeV/c])^2 \tag{2.25}$$

illustrated on figure 2.4.b.

## 2.5 Total Lifetime

Assuming that cooling prevents the blow up due to multiple scattering, only nuclear and single Coulomb scattering contribute to beam loss. As they both lead to exponential decays, we can calculate the total beam lifetime as

$$\tau_{n+sc} = \left(\tau_n^{-1} + \tau_{sc}^{-1}\right)^{-1} \tag{2.26}$$

a plot of which is shown in figure 2.5.

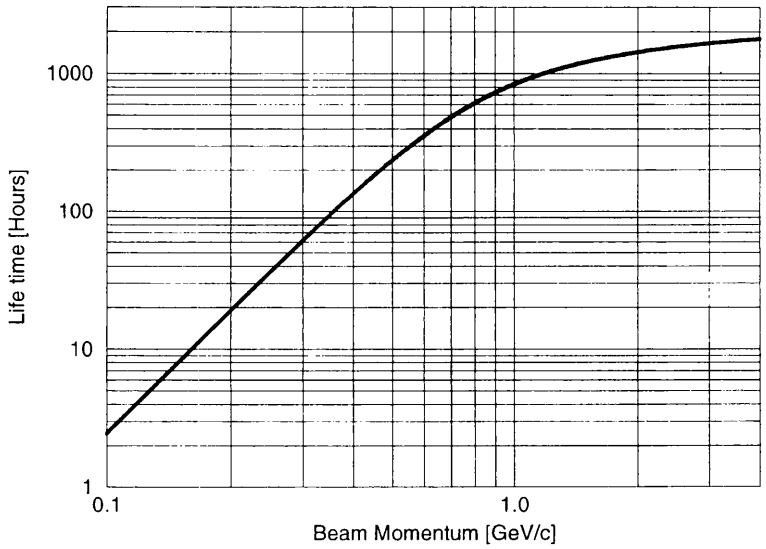


Figure 2.5: Total lifetime (without beam blow-up) caused by single and nuclear scattering for the AD with standard vacuum conditions.

Comparing these results with the time it takes for the uncooled beam to start being scraped by the aperture of the vacuum chamber (figure 2.4.b) it is clear that for the uncooled beam multiple scattering will dominate the losses at low energies. Only at energies above approximately 1 GeV the influence from nuclear and single Coulomb scattering starts to be of same order of magnitude as the losses induced by multiple scattering.

But in order to compare the multiple scattering results directly with the nuclear and single Coulomb scattering, we need to extract the time behavior of the multiple scattering losses in order to establish the $1/e$ lifetime from the emittance growth.

The $2\sigma$ emittance growth was given in equation (2.23). If we assume a Gaussian distribution of particles in each transverse phase space, and choose a coordinate system, where the particle motion in phase space is a circle, we can estimate the fraction $\eta$ of particles within the acceptance as follows :

$$\eta(t) = \frac{1}{(\sigma_z(t))^2} \int_0^{r_{accep}} \exp\left(-\frac{-r^2}{2(\sigma_z(t))^2}\right) r dr$$

$$= 1 - \exp(-\frac{r^2_{accep}}{2(\sigma_z(t))^2})$$
$$= 1 - \exp(-\frac{\epsilon_{accep}}{2(\epsilon_{2,z}(t)/4)}) \quad (2.27)$$

which using the above numbers results in the behaviour illustrated in figure 2.6.

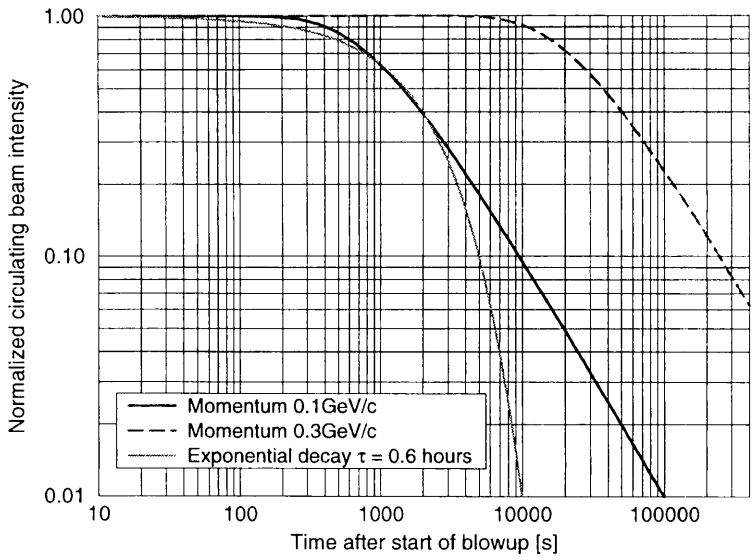


Figure 2.6: Calculation of the normalized beam intensity left in the AD, assuming standard AD vacuum conditions, as a function of time, when only losses induced by multiple scattering are taken into account (initial emittance 6 $\pi$ mm mrad). The exponential decay shown is the approximation used for the lifetime calculations.

The behaviour is clearly not an exponential decay, but as the exponential decay is faster than the decay due to multiple scattering, we can make a lower limit estimate on the lifetime of the beam as a function of energy by approximating the behaviour with an exponential decay. We do this by calculating the time at which the intensity has fallen to a fraction $e^{-1}$, i.e.

$$\tau_{ms} = \frac{-2\epsilon_{accep}/\ln(1-e^{-1}) - \epsilon_{init,2\sigma}}{3.17 \cdot 10^{-4}\ \pi \text{ mm mrad}} \cdot \beta(p[\text{Gev/c}])^2 \cdot \text{s}$$
$$= 27.6 \text{ hours} \cdot \beta(p[\text{GeV/c}])^2 \quad (2.28)$$

where we have used $\epsilon_{init,2\sigma} = 6\ \pi$ mm mrad. We note that for the AD the 'lifetime' (equation (2.28)) is a factor of 3 longer than the $t_{scraped}$ (equation (2.25)) for the 'beginning' of the losses. The lifetime (equation (2.28)) has been plotted as function of energy as the dashed curve on figure 2.7. It is an approximation to use $6\pi$ mm mrad as the initial emittance independent of energy, but as the acceptance is rather large the estimate is reasonable for

the low energies where we have the shortest lifetimes. Combining this estimate with the lifetime calculations for nuclear and single Coulomb scattering we obtain the lifetime for an uncooled beam in the AD as a function of the beam energy. A plot of this is shown in figure 2.7.

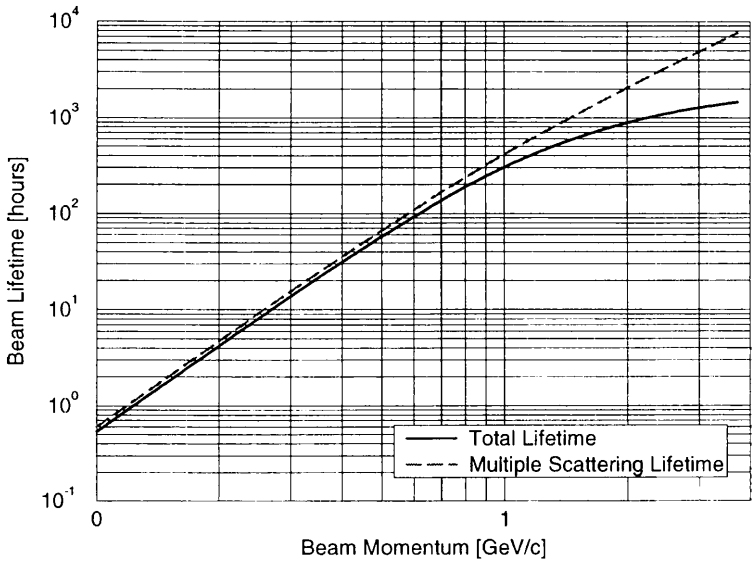


Figure 2.7: Lifetime of an uncooled circulating beam in the AD, including all contributions from multiple scattering (beam blow up), nuclear scattering and single Coulomb scattering.

Keeping in mind that the plot in figure 2.7 is log-log we observe that at approximately 2 GeV the contribution from multiple scattering and the contributions from nuclear and single Coulomb scattering are equal. Thus as expected multiple scattering dominates for low energies, and it is at the high energies that the direct losses become important. It should however also be noted that in the range where the different contributions are the same order of magnitude, the lifetime is rather long compared with the expected cycle times of the AD (figure 1.1).

## 2.6 Dependence on vacuum composition

An interesting question is how much the changes in vacuum composition alters the results. A simple estimate can be done by using the different measured compositions already at hand [10]. The measurements are listed (converted into densities) in table A.3 in appendix A. In table 2.1 are given the corresponding effective densities for the different loss mechanisms.

The last row in table 2.1 shows the range of deviations from the "standard vacuum description" used in the rest of this text. The largest variations seems to be on the multiple

| Density type. | Dens No.1 [$m^{-3}$] | Dens No.2 [$m^{-3}$] | Dens No.3 [$m^{-3}$] | Dens No.4 [$m^{-3}$] |
|---|---|---|---|---|
| $n_{ms}$ | $5.50 \cdot 10^{15}$ | $6.79 \cdot 10^{15}$ | $5.67 \cdot 10^{15}$ | $7.02 \cdot 10^{15}$ |
| $n_{ns}$ | $1.29 \cdot 10^{15}$ | $1.41 \cdot 10^{15}$ | $1.28 \cdot 10^{15}$ | $1.38 \cdot 10^{15}$ |
| $n_{sc}$ | $6.35 \cdot 10^{15}$ | $7.87 \cdot 10^{15}$ | $6.57 \cdot 10^{15}$ | $8.16 \cdot 10^{15}$ |
| Dev. from No.1 | - | 9% - 24% | 1% - 3.5% | 7% - 31% |

Table 2.1: Effective densities for the compositions listed in table A.3. For these densities the AC pressure of $8 \cdot 10^{-7}$ Pa was assumed.

scattering and the single Coulomb scattering densities, this is because these both scale with $Z^2$ whereas the nuclear scattering scales only with $A^{2/3}$. As the multiple scattering dominates for small energies and the nuclear for high energies, the variations in the single Coulomb scattering probability will not influence the losses much. Thus in the worst case we can expect the lifetime in the low energy range to be $\sim$ 30% less than the estimates otherwise given here, and in the high energy range $\sim$ 15% less.

## 2.7 Comparison with AC measurements

Before the shut down of the AC a few measurements of the beam lifetime as a function of energy were done [11], these should give us a clue as to how good the approximations done in the previous sections are. Figure 2.8 shows the results plotted together with estimates calculated from the equations in the present note.

The small deviations between the measured points, which themselves hold an unknown uncertainty, and the theoretical estimates, indicates that the validity of the calculations is rather good. The theoretical estimate has been made using the standard vacuum composition (appendix A).

## 2.8 Blowup during deceleration

During the last deceleration phase from 0.3 GeV/c to 0.1 GeV/c the assumptions have so far been that the emittance after blow up will be mainly due to the adiabatic blow up. Thus in the design study, the influence from vacuum has been ignored (see table 1.1). We derive in this chapter an expression for the blow up due to multiple scattering as a function of energy. Using this expression together with the adiabatic blow up, we can calculate the expected emittance after deceleration. The growth rate of the emittance is given by (equation (2.23))

$$\frac{\partial \epsilon}{\partial t}(p) = 2\pi\beta_z n_{ms} C_{ms} r_e^2 \frac{(m_e c^2)^2}{\beta c p^2} \tag{2.29}$$

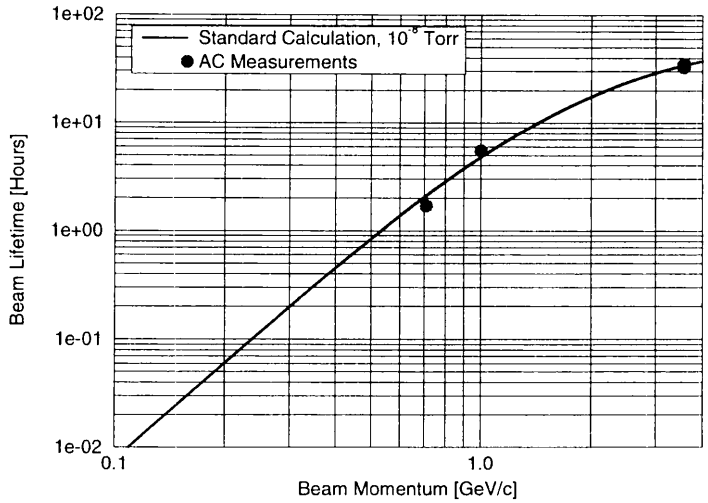


Figure 2.8: Comparison between the AC lifetime measurements and the results from these notes. It should be noted that the AC has a slightly different beta function average than the AD, this has not been taken into account. The densities were scaled to a $N_2$ equivalent pressure of $1.0{\cdot}10^{-8}$ Torr = $1.3{\cdot}10^{-6}$ Pa. to coincide with the actual AC pressure during the lifetime measurements [11]. Standard vacuum composition (appendix A) was used.

In figure 2.9 the additional emittance due to multiple scattering after deceleration as a function of the time spent on the deceleration process in shown. The calculation was done by integration the blowup of the invariant emittance (as also shown in [13]):

$$\Delta\epsilon(t_{decel}) = \frac{1}{\beta_f\gamma_f}\int_0^{t_{decel}} \frac{\partial\epsilon}{\partial t}(p)\,\beta\gamma\,dt \tag{2.30}$$

where $\beta_f$ and $\gamma_f$ are the final relativistic factors (at 0.1 GeV/c in this case), and the momentum $p$ depends on time.

## 2.9 Conclusions

As mentioned in [2] it is clear that for low energies the lifetime in the AD is dominated by multiple scattering in the uncooled case. The desired factor 20 improvement of the vacuum gives us however an emittance blow up rate at 0.1 GeV/c of $\sim 0.3\ \pi$ mm mrad/s, which with the expected electron cooling time of 1 second given in the design report [1], will result in an equilibrium emittance of $\sim 0.3\ \pi$ mm mrad better than the aim of $1\ \pi$ mm mrad. The vacuum composition is however also important, as up to 30% variations might occur for the same Nitrogen equivalent pressure, thus in worst case the equilibrium emittance about may increase to $\sim 0.4\ \pi$ mm mrad. However, as the vacuum improvement itself relies on doing some baking, which will automatically lower the average mass of the

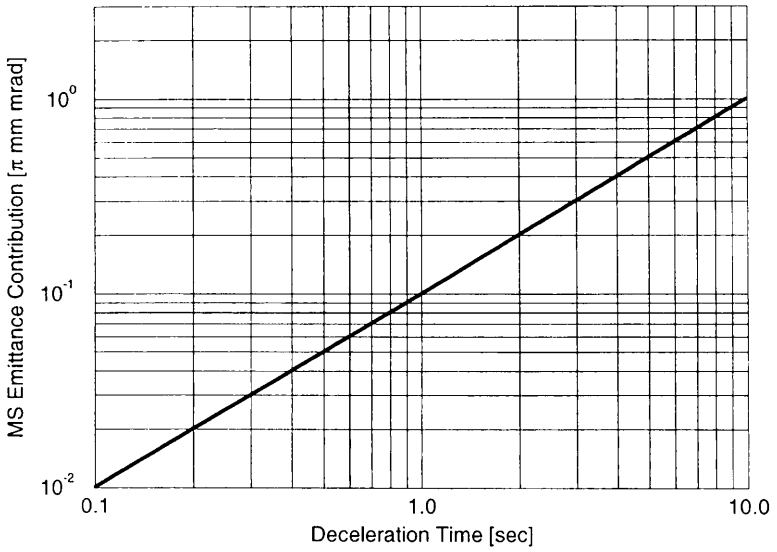


Figure 2.9: The change in emittance due to multiple scattering on rest gas during deceleration as a function of the time spent on the deceleration. For the calculation the AD vacuum conditions were used.

vacuum particles, this will improve together with the direct improvement from the average pressure drop.

The beam lifetime measurements in the AC turned out to be in rather good agreement with the theoretical values calculated using the observed pressure and the standard vacuum composition (Number 1, appendix A), which shows promise for the use of these calculations for predicting the conditions in the AD.

Studying the blowup due to multiple scattering on the rest gas we found that for the proposed deceleration time of 0.5s the contribution would be approximately 0.05 $\pi$ mm mrad. However, the 0.5s deceleration time is a bit optimistic, and will probably be more of the order 1-2 sec [12]. In that case $\Delta\epsilon$ is of order $0.2\pi$ mm mrad or about 5% of the adiabatic blow up. Thus the blowup due to multiple scattering for the expected deceleration times is not severe compared to the adiabatic contribution.

# Chapter III

# Intra Beam Scattering

In dense and low energy beams the effects from intra beam scattering are the most pronounced, thus in the AD where one requires a rather small final emittance at the last low energy flattop (just before extraction at 0.1 GeV/c) intra beam scattering (IBS) might give an important contribution to the equilibrium beam properties. Therefore this chapter is dedicated to a discussion of the magnitude and scaling of the intra beam scattering in the stored anti-proton beam in the AD.

## 3.1 Introduction

In the previous chapter we studied the beam lifetime and transverse blow up due to the interaction with the rest gas. In order to complete the study we examine in the present chapter the interaction between the beam particles. This interaction leads to a diffusion due to multiple Coulomb scattering between the beam particles as well as to friction.

As one of our purposes is to develop a simple set of equations for the beam development and equilibrium state, we would like to have the intra beam scattering contribution in an analytic form which can be used together with analytical expressions for the interaction with the residual gas and the influence of electron cooling. However, earlier studies have led to the construction of an intra beam scattering code [15] which calculates the growth rates and outputs them in a discrete form. As this code has been used and verified to some extent [16] we first give a short introduction to this code, and then present some simple analytical calculations of the diffusion and friction of intra beam scattering, which we verify with the IBS code.

## 3.2 Detailed approach

In earlier work summarized by M. Martini [14] intra beam scattering has been studied from a single particle point of view, calculating from first principles the interaction between charged particles in a beam in an accelerator. These calculations were later [15] implemented into a computer code INTRAB for calculations of beam emittance growth

rates and equilibrium conditions in different accelerators. The code was further improved in 1996 [16] in order to better include the lattice influence on the dynamics.

Using the code INTRAB with the parameters in table 3.1 we have calculated the expected emittance growth times due to intra beam scattering (ibs) for relevant energies, emittances and energy spreads.

| Parameter | Value |
|---|---|
| Beam Momentum | 0.3 to 0.1 GeV/c |
| $\Delta$p/p | $1{\cdot}10^{-5}$ to $1{\cdot}10^{-3}$ |
| Horizontal Tune | 5.39 |
| Vertical Tune | 5.37 |
| Number of particles | $5.0{\cdot}10^{7}$ |
| DTRINT (resolution) | $1.0{\cdot}10^{-12}$ |

Table 3.1: Typical input value ranges for INTRAB for AD intra beam scattering calculation

The program INTRABT generates the growth times for given emittances and energy spread. The growth times are defined as the growth time of the amplitudes, thus :

$$\tau_{x,y} = \frac{1}{\sigma_{x,y}} \frac{\partial \sigma_{x,y}}{\partial t} \tag{3.1}$$

$$\tau_{s} = \frac{1}{\sigma_{s}} \frac{\partial \sigma_{s}}{\partial t} \tag{3.2}$$

$$\tag{3.3}$$

where $\sigma_s$ is the spread of the momentum distribution, and all distributions are assumed Gaussian.

A series of different calculations has been done, and these have been compared to the similar calculation done with the analytical method described in the next section. To save space we show the results from using this program in the next section.

## 3.3 The simple approach

A different approach consists of viewing the beam as an infinitely long continuous plasma and use the Boltzmann transport equation including the collision term to calculate the diffusion and friction contributions. In this approach we thus ignore all alternating gradient effects and only use the average focusing force given by the betatron tune. I.e. we ignore coupling between the degrees of freedom induced by the lattice, this includes the coupling of the collective motion into the center of mass motion due to dispersion. Following the initial steps done in [18] in this direction we can, write the full transport equation as

$$\frac{df(\mathbf{v}.t)}{dt} = \frac{\partial f(\mathbf{v},t)}{\partial t} + \nabla_{\mathbf{v}}(f(\mathbf{v},t) \cdot \frac{\mathbf{F}(\mathbf{v})}{m_p}) \tag{3.4}$$

Here the left hand side is the collision term, which in this context describes in-plasma collisions. The force term **F** is the sum of external forces on the plasma. Now, if we want to include the diffusion induced by the rest gas, it can be done as described in [18]

$$\frac{\partial f}{\partial t} = \frac{\partial}{\partial v_\perp}\left(-F_{ecool,\perp}(v_\perp)f(v_\perp) + D\frac{\partial f}{\partial v_\perp}\right) \tag{3.5}$$

The collision term can, in the small angle approximation, be expressed as [18]

$$\frac{df(\mathbf{v},t)}{dt} = -\nabla_{\mathbf{v}}\cdot\mathbf{s} = -\frac{\partial s_\alpha}{\partial v_\alpha} \tag{3.6}$$

where **s** is the particle flux in momentum space. This flux can via the principle of detailed balance and the small angle approximation be found to be [18]

$$s_\alpha = \frac{n_p e^4 L_p}{8\pi\epsilon_0^2 m_p^2}\int\left(f\frac{\partial f'}{\partial v'_\beta} - f'\frac{\partial f}{\partial v_\beta}\right)\frac{(\mathbf{v}-\mathbf{v}')^2\delta_{\alpha\beta} - (v_\alpha - v'_\alpha)(v_\beta - v'_\beta)}{|\mathbf{v}-\mathbf{v}'|^3}d^3v' \tag{3.7}$$

where $L_p$ is the Coulomb logarithm for (anti) protons. There are two fundamentally different terms in this expression, the first term has the behavior of a friction force (compare it to the friction term in equation (3.4)), whereas the second has a diffusion like behavior. The Coulomb Logarithm is given by

$$L_p = \ln\left[\frac{4\pi v_{p,\perp}^3}{\sqrt{n_p}}\left(\frac{\epsilon_0 m_p}{e^2}\right)^{3/2}\right] \tag{3.8}$$

where $n_p$ is the ring averaged proton density, given by

$$n_p = \frac{N_p(\beta c)^2}{C\pi\beta_z^2 v_{p,\perp}^2} \tag{3.9}$$

In equation (3.9) $\beta$ is the relativistic factor of the beam longitudinal motion, and $\beta_z$ is the ring averaged beta function. Thus we choose to ignore the variations in particle density due to the alternating gradient lattice.

Now in order to compare this to the single particle approach we have to calculate the two contributions.

### 3.3.1 Diffusion in the anti-proton plasma

The diffusion part of equation (3.7) can be written as

$$s_\alpha^{diff} = -\frac{n_p e^4 L_p}{8\pi\epsilon_0^2 m_p^2}\int f'\frac{\partial f}{\partial v_\beta}\frac{(\mathbf{v}-\mathbf{v}')^2\delta_{\alpha\beta} - (v_\alpha - v'_\alpha)(v_\beta - v'_\beta)}{|\mathbf{v}-\mathbf{v}'|^3}d^3v' \tag{3.10}$$

and if we choose to ignore velocity dependence of $s_\alpha^{diff}$, we can define a velocity independent diffusion coefficient

$$\frac{df(\mathbf{v},t)}{dt} = D_{\alpha\beta}\frac{\partial^2 f(\mathbf{v},t)}{\partial v_\alpha \partial v_\beta} \tag{3.11}$$

where

$$D_{\alpha\beta} = \frac{n_p e^4 L_p}{8\pi\epsilon_0^2 m_p^2} \int f(\mathbf{v}', t) \frac{(\mathbf{v}')^2 \delta_{\alpha\beta} - (v'_\alpha)(v'_\beta)}{|\mathbf{v}'|^3} d^3v' \tag{3 12}$$

we will furthermore do the approximation that there is no coupling between the three degrees of freedom (not unrealistic as our proton beam is not very dense, and we have ignored lattice effects).

### Transverse Diffusion

For simplicity we will assume that the transverse velocity spread is isotropic. For the transverse dimensions we obtain the following expression

$$\frac{df(v_\perp, t)}{dt} = (D_{xx} + D_{zz}) \frac{\partial^2 f(v_\perp, t)}{\partial v_\perp^2} = D_\perp \frac{\partial^2 f(v_\perp, t)}{\partial v_\perp^2} \tag{3.13}$$

where

$$D_{xx,zz} = \frac{n_p e^4 L_p}{8\pi\epsilon_0^2 m_p^2} \int f(\mathbf{v}', t) \frac{(\mathbf{v}')^2 - {v'_{x,z}}^2}{|\mathbf{v}'|^3} d^3v' \tag{3.14}$$

as the longitudinal electron temperature is more than an order of magnitude lower than the transverse, we will choose to assume the same for the beam temperatures, we can thus approximate $D_\perp$ to be

$$D_\perp = \frac{n_p e^4 L_p}{8\pi\epsilon_0^2 m_p^2} \int_0^\infty f(v'_\perp, t) 2\pi dv'_\perp \tag{3.15}$$

assuming a Gaussian distribution, we obtain

$$D_\perp^{plas} = \frac{n_p e^4 L_p}{8\sqrt{2\pi}\epsilon_0^2 m_p^2 \sigma_\perp} \tag{3.16}$$

which should be included in the total diffusion. As we are only considering one transverse plane at a time, the diffusion in each plane is $D_z = \frac{1}{2} D_\perp$.

If we for a moment only consider the diffusion contribution, we know that the transverse velocity spread will change as

$$\langle v^2 \rangle = 2Dt \tag{3.17}$$

the growth rate from INTRABT is the amplitude growth rate, thus we calculate

$$\frac{\partial \sigma_{v_\perp}^2}{\partial t} = 2\sigma_{v_\perp} \frac{\partial \sigma_{v_\perp}}{\partial t} = 2D \tag{3.18}$$

where $\tau_\perp$ is given by

$$\tau_\perp = \left( \frac{1}{\sigma_{v_\perp}} \frac{\partial \sigma_{v_\perp}}{\partial t} \right)^{-1} = \frac{\sigma_{v_\perp}^2}{D} = \frac{\epsilon_\perp (\beta c)^2}{\beta_\perp D_\perp} \tag{3.19}$$

Longitudinal Diffusion

As the longitudinal acceptance also might be a limiting factor, we are also interested in the longitudinal diffusion coefficient. Using the general result from before we obtain

$$D_{ss} = \frac{n_p e^4 L_p}{8\pi\epsilon_0^2 m_p^2} \int f(\mathbf{v}', t) \frac{v_x'^2 + v_z'^2}{|\mathbf{v}'|^3} d^3v' \tag{3.20}$$

assuming again that the transverse dimension is much warmer than the longitudinal, we can by using polar coordinates find

$$\begin{aligned} D_{ss} &= \frac{n_p e^4 L_p}{8\pi\epsilon_0^2 m_p^2} \left( \frac{1}{(2\pi)^{3/2}\sigma_\perp^2 \sigma_\parallel} \right) \int_{-\infty}^{\infty} \int_0^{\infty} e^{-\frac{v_\perp'^2}{2\sigma_\perp^2} - \frac{v_\parallel'^2}{2\sigma_\parallel^2}} \frac{v_\perp'^2}{\left[v_\perp'^2 + v_\parallel'^2\right]^{3/2}} 2\pi v_\perp' dv_\perp' dv_\parallel' \\ &= \frac{n_p e^4 L_p}{8\pi\epsilon_0^2 m_p^2} \frac{1}{(2\pi)^{1/2}\sigma_\perp^2 \sigma_\parallel} \int_0^{\infty} \int_0^{\pi} e^{-\frac{v'^2}{2\sigma_\parallel^2}\left(\cos^2\theta + (\frac{\sigma_\parallel}{\sigma_\perp})^2 \sin^2\theta\right)} \sin^3\theta v' d\theta dv' \\ &= \frac{n_p e^4 L_p}{8\pi\epsilon_0^2 m_p^2} \frac{\sigma_\parallel^2}{(2\pi)^{1/2}\sigma_\perp^2 \sigma_\parallel} \int_0^{\pi} \frac{\sin^3\theta}{\cos^2\theta + \frac{T_\parallel}{T_\perp}\sin^2\theta} d\theta \end{aligned} \tag{3.21}$$

the integral evaluates as

$$\int_0^{\pi} \frac{\sin^3\theta}{\cos^2\theta + \frac{\sigma_\parallel^2}{\sigma_\perp^2}\sin^2\theta} d\theta \approx \int_0^{\pi} \frac{1}{\cot^2(\theta) + \frac{\sigma_\parallel^2}{\sigma_\perp^2}} d\theta \approx 2\frac{\sigma_\perp}{\sigma_\parallel} \mathrm{atan}(\pi/2\frac{\sigma_\perp}{\sigma_\parallel}) \tag{3.22}$$

thus

$$D_{ss} = \frac{n_p e^4 L_p}{8(2\pi)^{1/2}\epsilon_0^2 m_p^2 \sigma_\perp} \tag{3.23}$$

here again we can find the amplitude growth rate as we did for the transverse emittance in equation (3.19)

$$\tau_s = \left( \frac{1}{\sigma_{v_s}} \frac{\partial \sigma_{v_s}}{\partial t} \right)^{-1} = \frac{\sigma_{v_s}^2}{D_{ss}} = \frac{(dp/p)^2 (\beta c)^2}{D_{ss}} \tag{3.24}$$

where according to [14] $(dp/p)^2 = \sigma_\eta^2$.

### 3.3.2 Friction in the anti-proton plasma

Now, to get the complete picture at low transverse temperatures (velocities), it is necessary to investigate the friction term of (3.7) also. The friction term can be written :

$$\begin{aligned} s_\alpha^{fric} &= \frac{n_p e^4 L_p}{8\pi\epsilon_0^2 \cdot m_p} f(\mathbf{v}, t) \int \frac{\partial f(\mathbf{v}', t)}{\partial v_\beta'} \frac{(\mathbf{v} - \mathbf{v}')^2 \delta_{\alpha\beta} - (v_\alpha - v_\alpha')(v_\beta - v_\beta')}{|\mathbf{v} - \mathbf{v}'|^3} d^3v' \\ &= -\frac{n_p e^4 L_p}{8\pi\epsilon_0^2 \cdot m_p} f(\mathbf{v}, t) \int 2f(\mathbf{v}', t) \frac{(v_\alpha - v_\alpha')}{|\mathbf{v} - \mathbf{v}'|^3} d^3v' \end{aligned} \tag{3.25}$$

where we have done one step of partial integration.

Considering how a friction force is included in the transport equation, we can now write the friction force due to friction internally in the anti proton plasma as

$$F^{fric}_{plasma,\alpha} = -\frac{n_p e^4 L_p}{4\pi\epsilon_0^2 \cdot m_p} \int f'(\mathbf{v}', t) \frac{(v_\alpha - v'_\alpha)}{|\mathbf{v} - \mathbf{v}'|^3} d^3v' \tag{3.26}$$

Now, we can also write the force as

$$\mathbf{F}^{fric}_{plasma} = \frac{n_p e^4 L_p}{4\pi\epsilon_0^2 \cdot m_p} \nabla_{\mathbf{v}} \int \frac{f'(\mathbf{v}', t)}{|\mathbf{v} - \mathbf{v}'|} d^3v' \tag{3.27}$$

this is very similar to the expression for the electric field in electrostatics. Thus we can apply Gauss' law, which states

$$\nabla \cdot \mathbf{E} = 4\pi\rho \tag{3.28}$$

where in this case the electric field is the integral in the expression for $\mathbf{F}$, and $\rho$ is the distribution function. Thus

$$\nabla \cdot \mathbf{F} = 4\pi f(\mathbf{v}, t) \frac{n_p e^4 L_p}{4\pi\epsilon_0^2 \cdot m_p} \tag{3.29}$$

leading to

$$2\frac{\partial F_z}{\partial v_z} = 4\pi f(\mathbf{v}, t) \frac{n_p e^4 L_p}{4\pi\epsilon_0^2 \cdot m_p} - \frac{\partial F_s}{\partial v_s} \tag{3.30}$$

unfortunately, by choosing the longitudinal velocity spread to be much smaller than the transverse, the derivative with respect to the longitudinal component will be much larger for small velocities than the transverse, thus making this approach useless. Here, however, we are mainly interested in getting an estimate to compare with the results from the single particle code. Thus we choose to select a longitudinal velocity spread of the same order as the transverse, and we obtain the following expression for the vertical as well as the longitudinal friction force

$$F^{plas}_{z,s}(v_{z,s}) = -v_{z,s} \frac{1}{3 \cdot (2\pi)^{3/2} \sigma_s \sigma_z^2} \frac{n_p e^4 L_p}{\epsilon_0^2 \cdot m_p} \tag{3.31}$$

which we can combine with the earlier derived diffusion coefficient, to obtain the growth rate due to intra beam scattering in the continuous approximation.

## 3.4 Calculations for the AD

We wish to know how the beam properties develop at the low energy plateaus and during deceleration from 0.3 GeV/c to 0.1 GeV/c. For this purpose it will be easier (and faster) to use the analytical formulas presented in the last section, but we need to know how well they reproduce the more accurate calculations of INTRABT. For this comparison we have

| Parameter | Value |
|---|---|
| Beam Momentum | 0.3 to 0.1 GeV/c |
| Average Horizontal Betafunction | 7.487 m |
| Average Vertical Betafunction | 6.575 m |
| Number of particles | $5.0{\cdot}10^7$ |
| AD Circumference | 182.43 m |

Table 3.2: Values used for the AD plasma diffusion calculation.

chosen several different settings relevant for the AD and calculated the growth times. In table 3.2 some relevant parameters for the AD have been listed.

Firstly we would like to know how the blowup rates depend on the transverse emittance. We chose for simplicity identical horizontal and vertical emittances. In figure 3.1 are shown the blow up rates for both the transverse and the longitudinal dimensions, calculated using both the INTRABT program and the analytical formulas derived in the last section. For the comparison we had to combine the diffusion and friction results, this was done by observing that [20]

$$\frac{d\langle v_{\perp,\parallel}^2\rangle}{dt} = \frac{2}{m_p} F_{\perp,\parallel}(v_{\perp,\parallel}) \cdot v_{\perp,\parallel} + 2D_{\perp,\parallel} \tag{3.32}$$

thus we defined an 'effective' diffusion coefficient for the growth rate calculations, this diffusion is given by

$$D_{\perp,\parallel}^{eff} = D_{\perp,\parallel} - \frac{v_{\perp,\parallel}}{m_p} F_{\perp,\parallel} \cdot \eta \tag{3.33}$$

where the fitting parameter $\eta$ has been introduced to compensate for differences between the result from the continuous calculation and the ibs program.

The correspondence between the two methods is good in the curves above, however the two values of the fitting parameters most likely compensates for the lack of taking the lattice into account in the analytical approach. Thus these would probably be different for other lattices/machines. But as we are mainly interested in modelling the physical processes responsible for the beam dynamics in a few simple cases the equations derived here constitute an adequate tool. However when sympathetic cooling becomes a dominant contribution the correspondence is unsatisfactory (differences up to a factor 10). This seems to suggest that the approximations done for the friction force are over optimistic. The basic assumption in these cases is that the longitudinal dimension is much colder than the transverse. This is clearly not the case for most of the situations expected for the AD.

Doing the same comparisons at 0.3 GeV/c reveals the same overall tendencies. Thus when heating is dominant we can use the analytical expressions, whereas in case of sympathetic cooling we must be careful, and turn to the ibs program (at least until a better expression for the friction force has been derived).

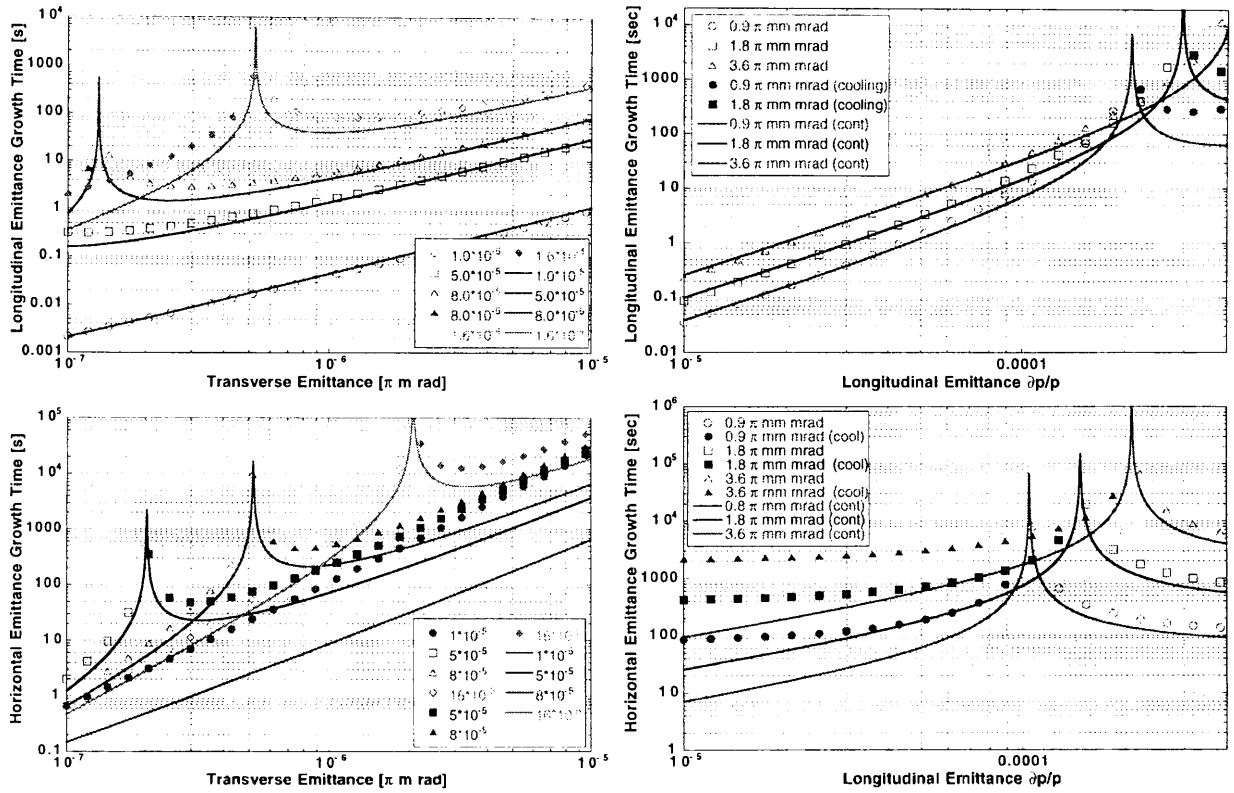


Figure 3.1: The figures show blowup rates at a momentum of 0.1 GeV/c. The point where the blowup changes to a cooling (sympathetic cooling) has been used to calibrate the friction force relative to the diffusion contribution. The isolated points are results from the ibs program whereas the lines are from the continuous calculation. Shown are the absolute values of the growth rates, cooling (negative growth rate) has been marked by solid data points. Top graphs (longitudinal) $\eta = 1.3$, bottom graphs (transverse) $\eta = 2.8^{-1}$

## 3.5 Blowup during deceleration

When the beam is decelerated from 0.3 GeV/c to 0.1 GeV/c the emittances blow up adiabatically, but due to IBS especially the longitudinal emittances is expected to suffer an additional increase. As there are limits to the longitudinal acceptance of the machine it is interesting to know how much blow up we can expect, and whether this is going to be a limiting factor for the experiments. To do this we need an estimate of the final emittances at 0.3 GeV/c before deceleration is started. For this we need the equilibrium with electron cooling, and as a first estimate we try with the values from the design report. These values were earlier shown in table 1.1.

A simple way of estimating the effect of the intra beam scattering is to first assume that there is no influence but the adiabatic blow up, and then calculate the growth rates for the different energies and beam characteristics. Figure 3.2 gives the growth rates for the different momenta, calculated under these assumptions.

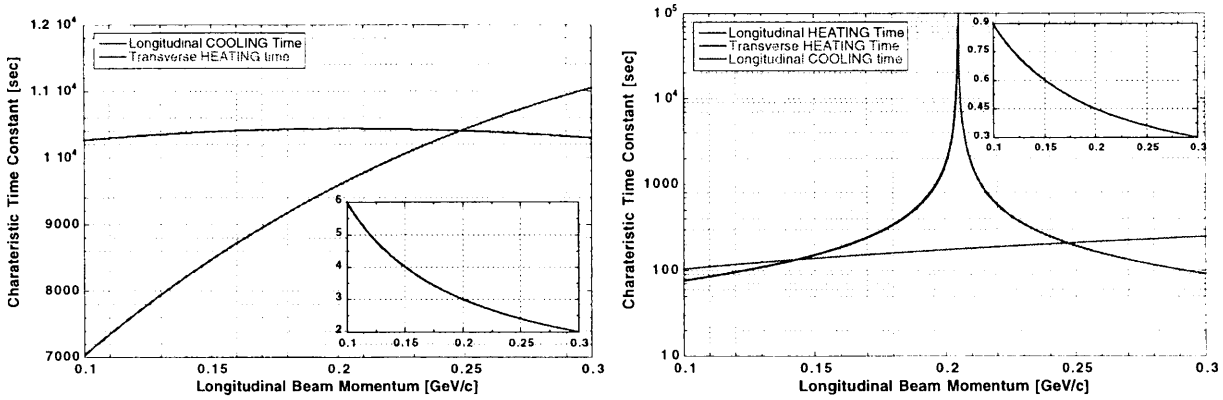


Figure 3.2: The left figure shows the longitudinal and transverse growth times for different energies, with emittances corresponding to the adiabatic blow up of the beam from the design rapport final emittances at 0.3 GeV/c. The figure on the right shows the growth times as expected if we assume a more efficient electron cooling at 0.3 GeV/c to values $\epsilon_\perp$ = 0.3 $\pi$ mm mrad and dp/p = $10^{-4}$. In both cases the inset shows the transverse emittance in $\pi$ mm mrad.

As seen on figure 3.2 it turns out that for the whole of the deceleration process the intra beam scattering growth times are long compared to the deceleration time, thus indicating small influence from intra beam scattering on the beam emittance and longitudinal velocity spread. This is valid even for the chosen cases with small equilibrium emittances at 0.3 GeV/c, and still much more pronounced for the design study case.

## 3.6 Conclusions

Generally the continuous plasma calculations match with the rather more involved calculations done in the intra beam scattering code INTRAB. The match is however fine tuned by fitting the balance point of the diffusion and friction forces to the results of INTRAB.

When sympathetic cooling becomes important the continuous calculations done here tends to predict too efficient cooling (or too little diffusion), thus these ranges should be used with care.

A quick look at the deceleration process suggests that the influence from intra beam scattering, for the standard particle number of $5{\cdot}10^7$ anti protons, is negligible. Thus it seems that we can ignore this contribution during deceleration, and only consider the adiabatic blowup and the blowup due to interaction with the rest gas as calculated in the last chapter.

# Chapter IV

# Conclusion

In this report we have studied some aspects of the physics determining how a beam of anti-protons will behave at low energy in the anti-proton decelerator (AD). We have concentrated on the influence of the residual gas on the beam lifetime as well as the beam emittance, and we have studied the intra-beam scattering by use of a computer code and, in order to understand the processes in the intra-beam scattering, we have developed some approximate analytical expressions describing how the emittance and momentum spreads are influenced by intra-beam scattering.

From the calculations on the beam interaction with the residual gas we found for the desired AD pressure of $3{\cdot}10^{-10}$ Torr that the lifetime of a cooled anti-proton beam (i.e. a beam that is prevented from blowing up and colliding with the aperture of the storage ring) was found to be of the order of 2.5 hours at 0.1 GeV/c, (see figure 1.1). The rate of emittance blow up without cooling was found to be 18 $\pi$ mm mrad/minute thus leaving room for alignment of electron cooling as well as debunching before cooling can be applied. Thus the estimates on the beam development due to interaction with the residual gas at the desired pressure showed that there is time for all planned operations.

A simple estimate of the blowup due to multiple scattering on the rest gas during the deceleration from 0.3 GeV/c to 0.1 GeV/c, showed that for a deceleration time of 0.5s the blowup would be of order 0.05 $\pi$ mm mrad, whereas for a more realistic deceleration time of 1-2s [12] the blowup would be of order 0.2 $\pi$ mm mrad. Compared to the adiabatic blowup from $2\pi$ mm mrad to 6 $\pi$ mm mrad the blowup due to scattering on the residual gas is small.

The approximate analytical intra-beam scattering calculations turned out to fit quite well with the more rigorous calculations of the computer code used for reference, once the simple calculations were fitted by used the balancing of the friction and diffusion processes in the beam. The calculations show that for the desired emittances and momentum spreads the intra-beam scattering growth during deceleration is not expected to add much compared to the adiabatic emittance growth.

In order to estimate what equilibrium beam can be obtained in the AD it is necessary also to consider the electron cooling applied at 0.3 GeV/c and 0.1 GeV/c. Electron cooling is however rather complicated to describe theoretically, thus in order to avoid too fast

conclusions we have omitted the first simple estimates from this report. However we can obtain a little information from the fact that the blowup rate due to multiple scattering on the residual gas at 0.1 GeV/c is expected to be of order 0.3 $\pi$ mm mrad/s, thus if we assume an electron cooling time of about 1 second [19] we would expect an equilibrium beam emittance of about 0.3 $\pi$ mm mrad, enough to adequate the design specifications.

All numbers given are for the design pressure ($3{\cdot}10^{-10}$ Torr) and the standard rest gas composition (Appendix A). If the corresponding vacuum conditions are not reached the setting up and performance of the machine may become critical.

# Appendix A

# Vacuum Conditions in the AC

As the cross section of the interaction between antiprotons and rest gas depends on the nature of the rest gas, the composition of the rest gas needs to be taken into account. Relevant numbers are given in table A.1.

| Spec. | Ion Gauge Cal. | RGA[1] Cal. | Composit. [arb. units] | Pressure $N_2$ eq. [Pa] | Pressure Abs [Pa] | Density [mol/m$^3$] | Density [%] |
|---|---|---|---|---|---|---|---|
| $H_2$ | 2.50 | 1.54 | 178 | $4.48{\cdot}10^{-7}$ | $1.12{\cdot}10^{-6}$ | $2.70{\cdot}10^{14}$ | 78.0 |
| $CH_4$ | 0.78 | 0.71 | 10 | $5.45{\cdot}10^{-8}$ | $4.25{\cdot}10^{-8}$ | $1.03{\cdot}10^{13}$ | 3.0 |
| $H_2O$ | 1.00 | 1.00 | 40 | $1.55{\cdot}10^{-7}$ | $1.54{\cdot}10^{-7}$ | $3.74{\cdot}10^{13}$ | 10.8 |
| CO | 0.83 | 1.00 | 35 | $1.36{\cdot}10^{-7}$ | $1.12{\cdot}10^{-7}$ | $2.71{\cdot}10^{13}$ | 7.8 |
| $N_2$ | 1.00 | 1.00 | 0 | 0 | 0 | 0 | 0.0 |
| Ar | 0.69 | 0.83 | 0 | 0 | 0 | 0 | 0.0 |
| $CO_2$ | 0.72 | 1.54 | 3 | $7.54{\cdot}10^{-9}$ | $5.43{\cdot}10^{-9}$ | $1.31{\cdot}10^{12}$ | 0.4 |

Table A.1: Residual gas description for the AC, $P_{IG,N_2} = 8.00{\cdot}10^{-7}$Pa (=$6.0{\cdot}10^{-9}$ Torr)

The calibrations of the Ion Gauge and the rest gas analyzer (RGA) are given in terms sensitivity to $N_2$ divided by the sensitivity to the gas in question. The pressure returned by a standard Ion Gauge is the Nitrogen equivalent pressure ($P_{IG,N_2}$).

As the relevant densities for the calculations are the atom densities, these have been listed in table A.2.

Table A.3 shows 4 different vacuum compositions, and the resulting effective densities (with which the lifetimes scale linearly). Measurement no.1 and 2. are measured in the AC. Measurement 3. and 4. are measured elsewhere, but in vacuum systems fairly equivalent to the conditions to be expected in the AC. Measurement no.4. is for a system where baking has not finished. All the measurements have been scaled to the same Nitrogen equivalent pressure (gauge reading).

[1]RGA: Rest Gas Analyzer

| Species | Atomic No. (A) | Charge (Z) | Density [atoms/$m^{-3}$] | $n_{ms}$ [$m^{-3}$] | $n_{ns}$ [$m^{-3}$] | $n_{sc}$ [$m^{-3}$] |
|---|---|---|---|---|---|---|
| H | 1 | 1 | $6.561 \cdot 10^{14}$ | $6.561 \cdot 10^{14}$ | $6.561 \cdot 10^{14}$ | $6.561 \cdot 10^{14}$ |
| C | 12 | 6 | $3.874 \cdot 10^{13}$ | $1.206 \cdot 10^{15}$ | $2.030 \cdot 10^{14}$ | $1.395 \cdot 10^{15}$ |
| N | 14 | 7 | 0 | 0 | 0 | 0 |
| O | 16 | 8 | $6.717 \cdot 10^{13}$ | $3.640 \cdot 10^{15}$ | $4.265 \cdot 10^{14}$ | $4.299 \cdot 10^{15}$ |
| Ar | 40 | 18 | 0 | 0 | 0 | 0 |

Table A.2: Atomic densities for the vacuum description in table A.1. The total multiple scattering density (eq. (2.20) is $n_{ms} = 5.50 \cdot 10^{15}$ $m^{-3}$. Total Hydrogen equivalent density (nuclear scattering, eq. (2.4)) $n_{ns} = 1.29 \cdot 10^{15}$ $m^{-3}$. Total single Coulomb scattering density (eq. (2.10)) $n_{sc} = 6.35 \cdot 10^{15}$ $m^{-3}$.

| Species | Dens No.1 [mol./$m^{-3}$] | Dens No.2 [mol./$m^{-3}$] | Dens No.3 [mol./$m^{-3}$] | Dens No.4 [mol./$m^{-3}$] |
|---|---|---|---|---|
| $H_2$ | $2.70 \cdot 10^{14}$ | $2.67 \cdot 10^{14}$ | $2.82 \cdot 10^{14}$ | $1.95 \cdot 10^{14}$ |
| $CH_4$ | $1.03 \cdot 10^{13}$ | $2.78 \cdot 10^{12}$ | $7.09 \cdot 10^{12}$ | $6.60 \cdot 10^{12}$ |
| $H_2O$ | $3.74 \cdot 10^{13}$ | $2.14 \cdot 10^{13}$ | $3.27 \cdot 10^{13}$ | $8.48 \cdot 10^{13}$ |
| CO | $2.72 \cdot 10^{13}$ | $4.64 \cdot 10^{13}$ | $2.67 \cdot 10^{13}$ | $1.46 \cdot 10^{13}$ |
| $N_2$ | 0 | 0 | $3.40 \cdot 10^{12}$ | $2.61 \cdot 10^{12}$ |
| Ar | 0 | 0 | $1.31 \cdot 10^{12}$ | 0 |
| $CO_2$ | $1.31 \cdot 10^{12}$ | $7.13 \cdot 10^{12}$ | $8.16 \cdot 10^{11}$ | $1.16 \cdot 10^{12}$ |
| | [$m^{-3}$] | [$m^{-3}$] | [$m^{-3}$] | [$m^{-3}$] |
| $n_{ms}$ | $5.50 \cdot 10^{15}$ | $6.79 \cdot 10^{15}$ | $5.66 \cdot 10^{15}$ | $7.02 \cdot 10^{15}$ |
| $n_n$ | $1.29 \cdot 10^{15}$ | $1.41 \cdot 10^{15}$ | $1.28 \cdot 10^{15}$ | $1.38 \cdot 10^{15}$ |
| $n_{sc}$ | $6.35 \cdot 10^{15}$ | $7.87 \cdot 10^{15}$ | $6.57 \cdot 10^{15}$ | $8.16 \cdot 10^{15}$ |

Table A.3: Results from different measurements of the vacuum composition. All cases have been normalized to a Nitrogen equivalent pressure of $8.0 \cdot 10^{-7}$ Pa. The No.1 densities are those used throughout the text.

# References


[1] "Design Study of the Antiproton Decelerator: AD", Edited by S. Maury, CERN PS 96-43 (AR).

[2] N. Madsen, in "Beam deterioration by multiple scattering on rest gas", CERN AD-Note 97-12.

[3] N. Madsen, O. Gröbner, S. Maury and D. Möhl, in "Beam Lifetime in the Antiproton Decelerator (AD)", CERN AD-Note 97-14.

[4] E. Fischer, in "Residual gas scattering...", CERN ISR-VAC/67-16.

[5] O. Gröbner and M. Brouet, in "Upgrading the AC vacuum system for the Antiproton Decelerator (AD)", CERN LHC, Vac. Tec. Note 97-06.

[6] D. Garetta *et al.*, in "Proceedings of the Third Lear Workshop", Tignes-Savoie-France, 599 (1985)

[7] P.J. Mulders, in "Proceedings of the Third Lear Workshop", Tignes-Savoie-France, 177 (1985)

[8] J.D. Jackson, in "Classical Electrodynamics", Second Edition, (Wiley, New York), (1975)

[9] K. Kilian and D. Möhl, CERN PS/DL/LEAR Note 81-1, *pp* LEAR Note 90 (1981)

[10] M. Brouet, CERN LHC/VAC, Private Communications (1997)

[11] T. Eriksson, CERN PS/OP, Private Communications (1997)

[12] F. Pedersen, CERN PS/RF, Private Communications (1998)

[13] W. Hardt, "A few simple expressions for checking vacuum requirements in a proton synchrotron", CERN ISR-300/GS/68-11.

[14] M. Martini, in "Intra beam Scattering", CERN PS/84-9 (AA).

[15] R. Giannini and D. Möhl, in "Intrab, a computer code to calculate growth rates, emittance evolution and equilibrium with intrabeam scattering and cooling", CERN PS/AR/Note 92-22.

[16] R. Giannini and D. Möhl, in "Improvements of intrabeam scattering codes intrab", CERN PS/AR/Note 96-19.

[17] M. Reiser, *Theory and Design of Charged Particle Beams* (Wiley, New York, 1994), Chap. 5. (1994)

[18] Landau and Lifshitz, in *Physical Kinetics*, vol 1, Pergamon (1981)

[19] D. Möhl, CERN PS/DI , Private Communications (1998)

[20] I.N. Meshkov, *Electron cooling: Status and perspectives*, Phys. Part. Nucl. **25**, 631 (1994)